# SUPRAMOLECULAR ORGANIC SEMICONDUCTING MATERIALS FOR OPTOELECTRONICS

## Acronim: SUPRAMOL-MAT

### Scientific Report STAGE 3 / 2024

## Code project: PN-III-P4-PCE-2021-0906

***PCE 120* din *14/06/2022***


**PROJECT MANAGER**

Dr. Aurica Farcas

**TEAM MEMBERS**

1. Dr. Ana-Maria Resmerita
2. Dr. Ursu Laura-Elena
3. Dr. Balan-Porcărașu Mihaela
4. Dr. Asăndulesa Mihai
5. Dr. Tigoianu Ionut Radu
6. Dr. Peptu Cristian

# Objectives/2024

W3.2. The synthesis of thiophene-phenylene-azomethine (TPA) and its inclusion complexes TPA/TMS·βCD,TPA/TMS·γCD,TPA/TMe·βCD, TPA/TMe·γCD and TPA/CB7;

W3.3. The synthesis of polyrotaxanes (PFTPA PRs) and the reference copolymer (PFTPA): Structural characterizations and photophysics by FTIR, NMR, GPC, TGA,

DSC, ESI-MS, UV-Vis, RAMAN and TEM;

W3.4. Electrochemical and morphological properties of PFTPA PRs and PFTPA;

W3.5. Electrical conductivities of PFTPA PRs and PFTA in their undoped and doped forms;

W3.6. Surface pressure-area isotherms and BAM studies of PFTPA PRs and PFTPA at the air/water interface;

W3.7. The testing in organic electronic devices: photovoltaics (PSCs) and other organic electronic devices

# W3.2. - 2024

The synthesis of thiophene-phenylene-azomethine (**3**) and its inclusion complex **3·TMe-βCD**

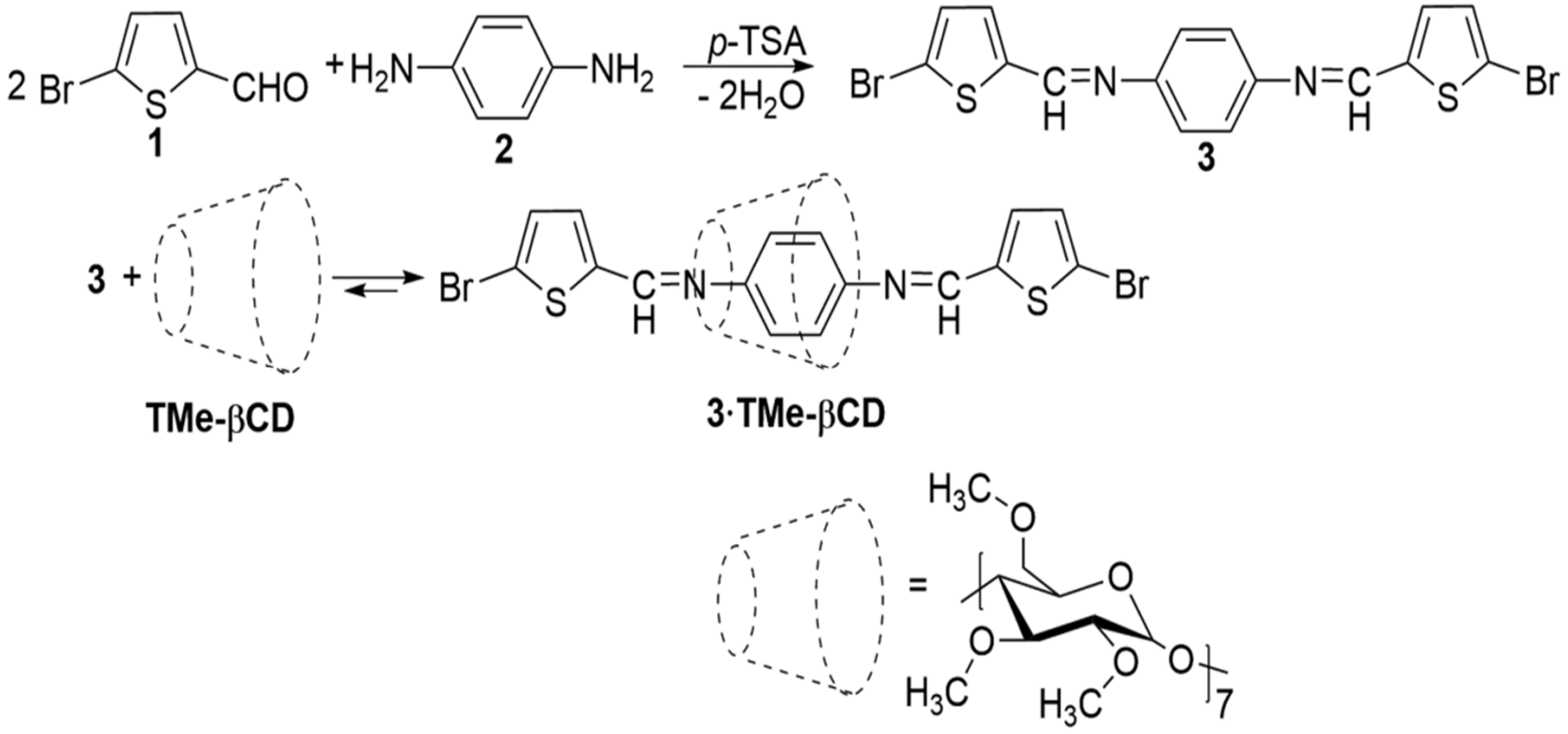


**Scheme 1**. Synthetic route to the target bisazomethine 3 and its encapsulated form 3·TMe-βCD.

# Structural characterization

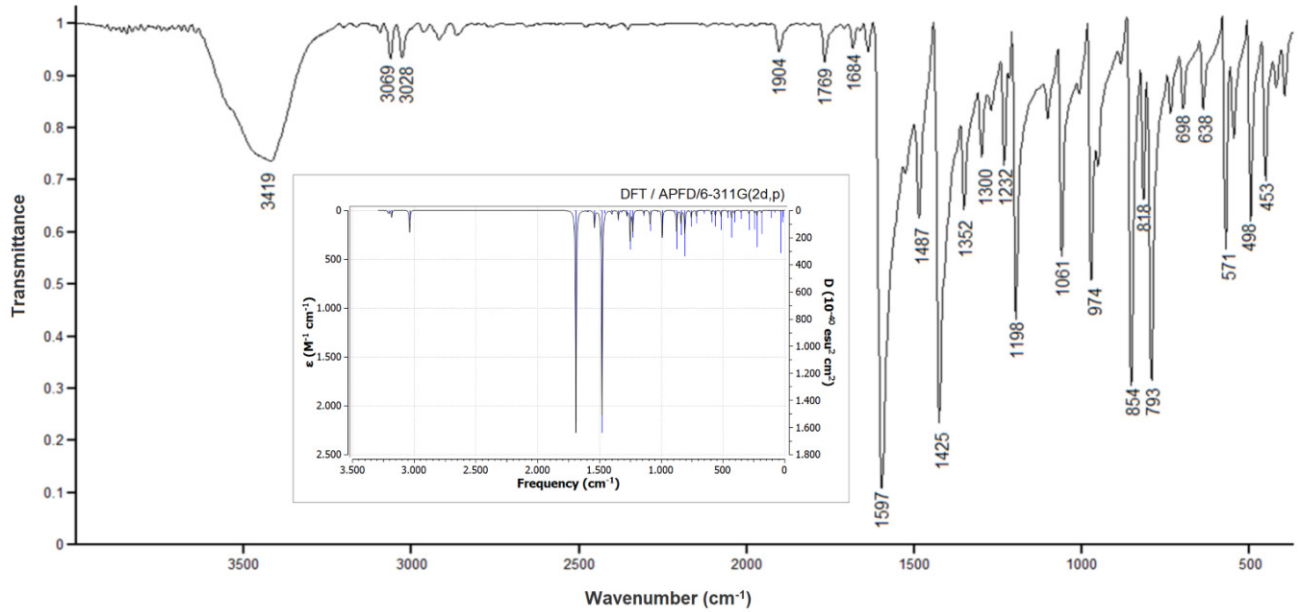


**Figure 1.** FT-IR spectrum correlated with DFT calculations of **3** bisazomethine.

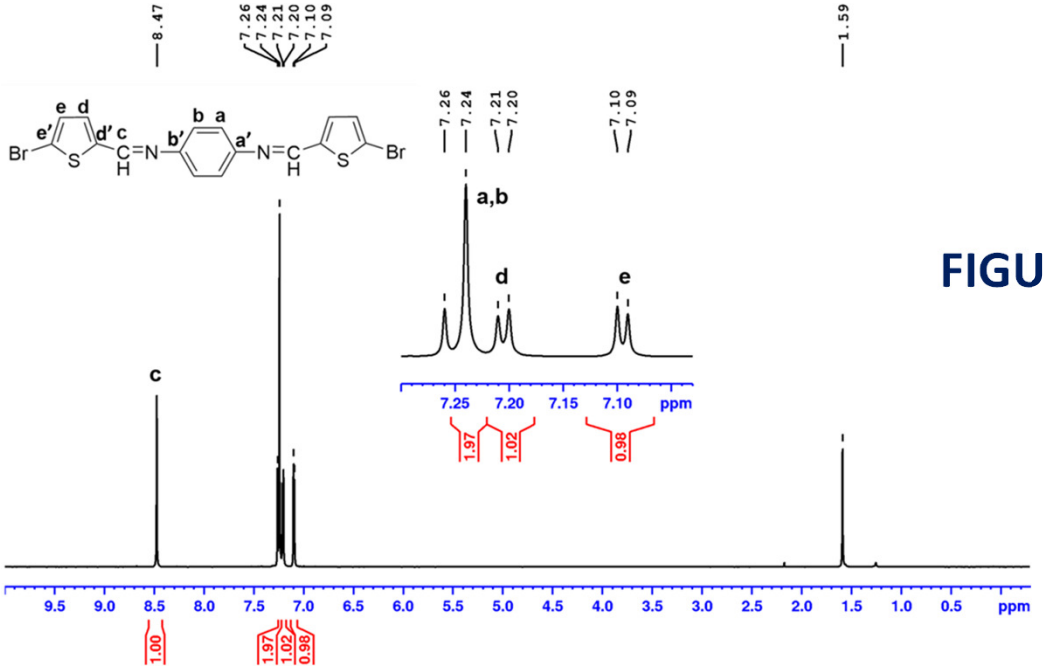


**FIGURE 2**. 1H-NMR spectrum of **3** in CDCl3.

# The host-guest complexation stoichiometry

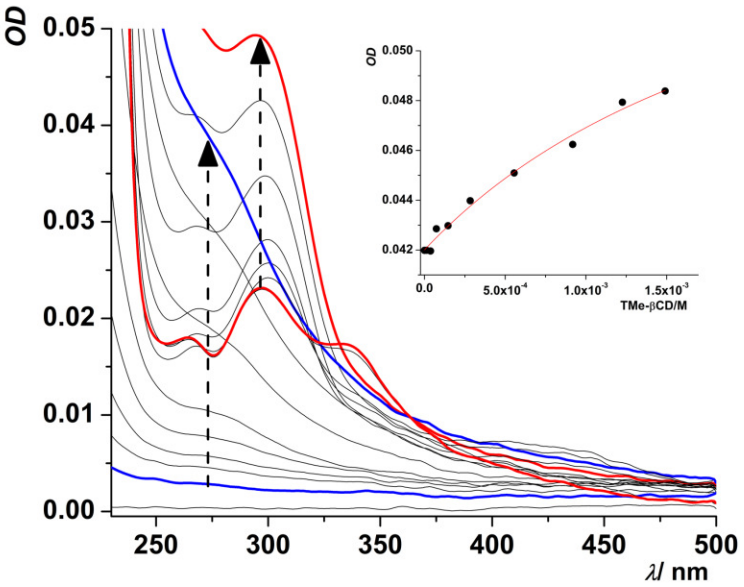


**Figure 3**. UV-Vis absorption titration of bisazomethine **3** monomer (1 μM solution in DCM) with increasing the concentration of TMe-βCD. The nonlinear fitting based on the UV-Vis absorption change assuming a 1:1 binding model, from which the association constant was derived.

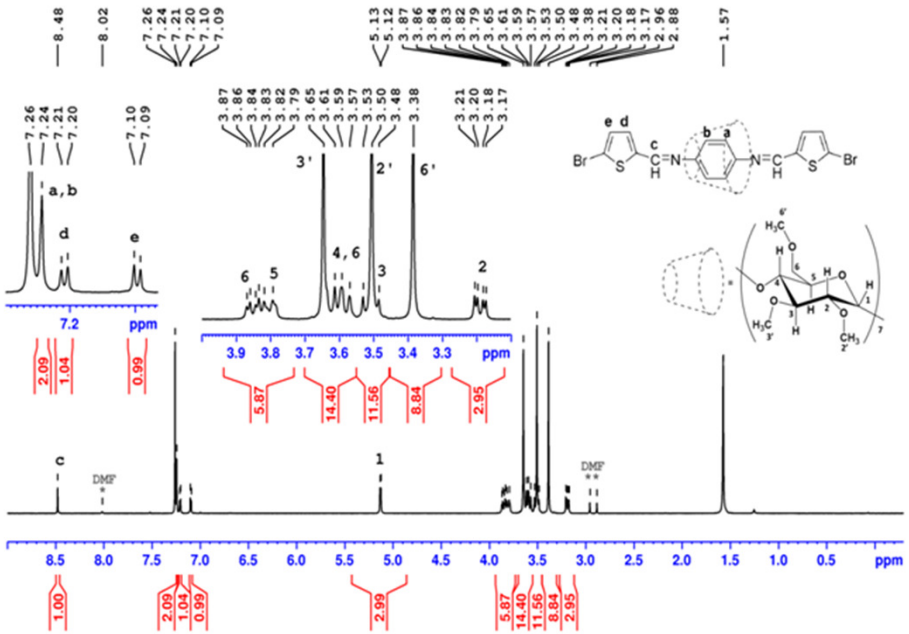


**Figure 4.** 1H-NMR spectrum of **3·TMe-βCD** in CDCl3.

## DFT computations for exploring electronic structure

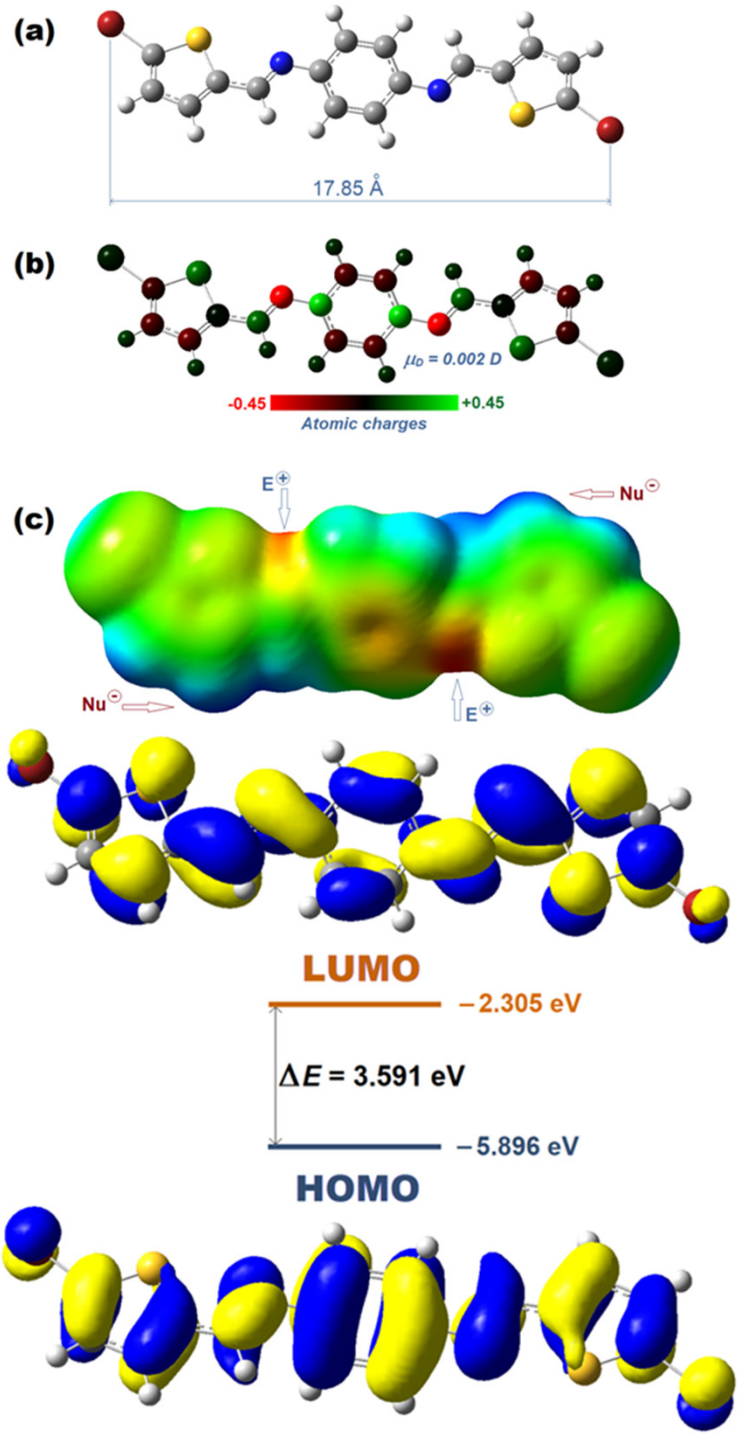


**Figure 5.** Molecular insights of compound **3**: Optimized geometry (conformation) by DFT method (a); distribution of partial atomic charges (Mulliken) and dipole moment value (b); electrostatic potential (c), represented as a mapped surface surrounding molecule 3, highlighting electrophilic attack sites (E+) and nucleophilic attack sites (Nu−); computation conducted at the APFD/6-311G(2d,p) theory level.

**Figure 6**. Frontier molecular orbital patterns (HOMO & LUMO) and corresponding band-gap energy value for compound **3**.

## Molecular docking simulation

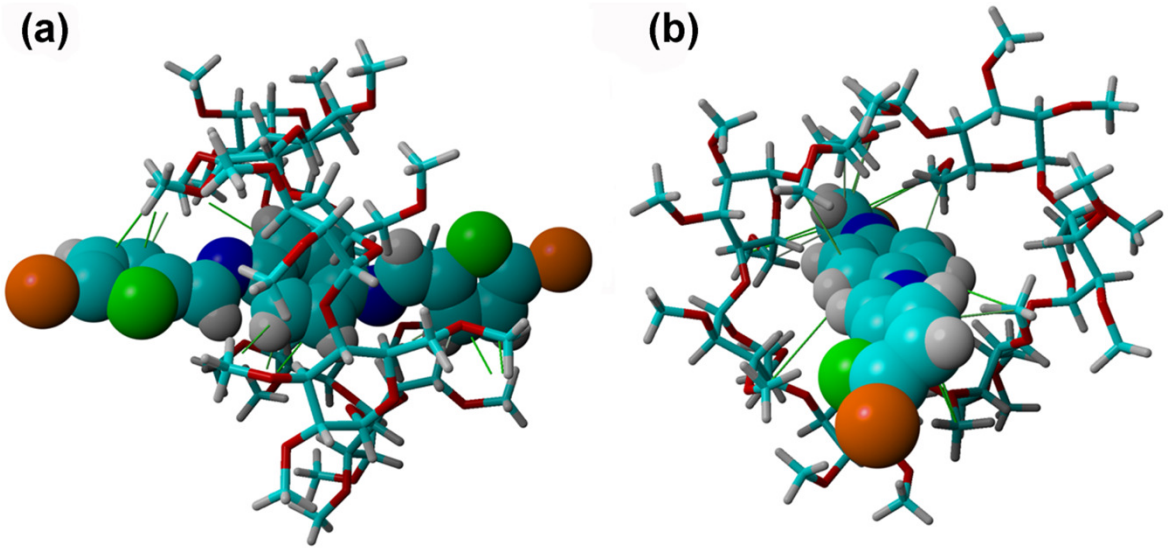


**Figure 7**. Molecular docking model of the best pose demonstrating inclusion complex formation between TMe-βCD (host) and molecule **3** (guest): (a) Side view of the **3·TMe-βCD** complex and (b) Top view of the **3·TMe-βCD** complex. Solid green lines are hydrophobic contacts.

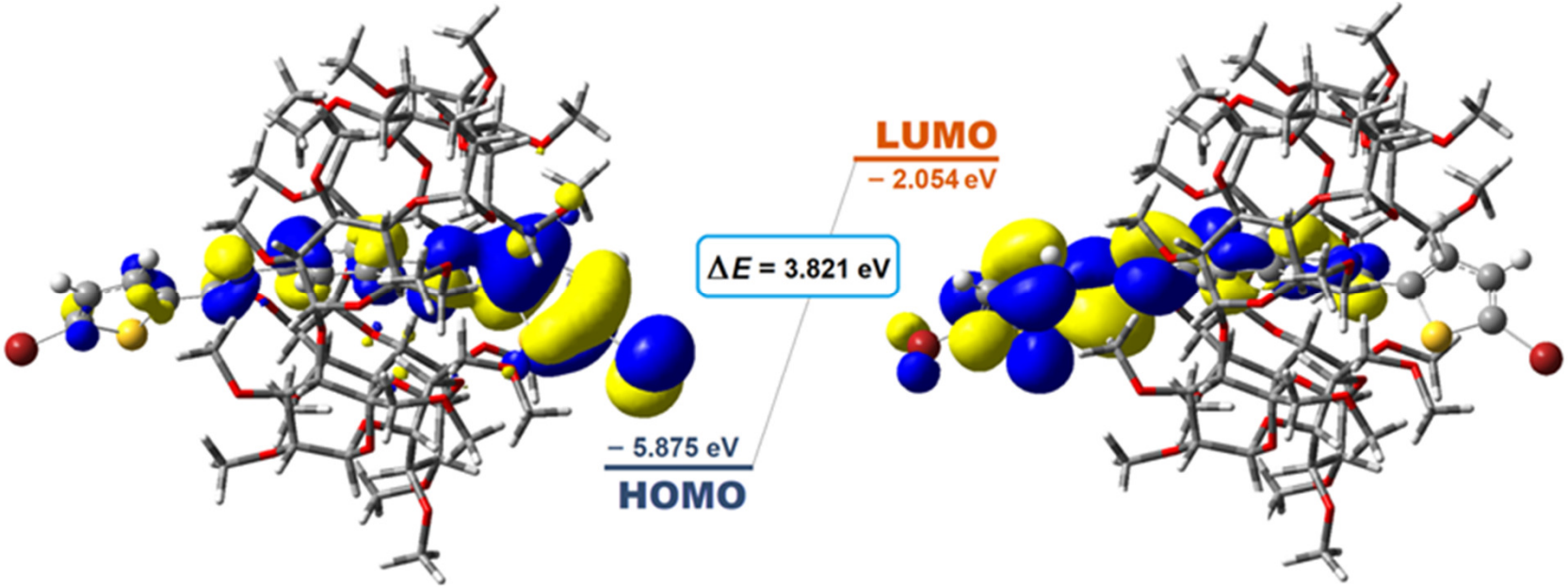


**Figure 8**. Frontier molecular orbital patterns (HOMO and LUMO) and corresponding band-gap energy value for the host-guest complex **3·TMe-βCD.**

## The surface morphology

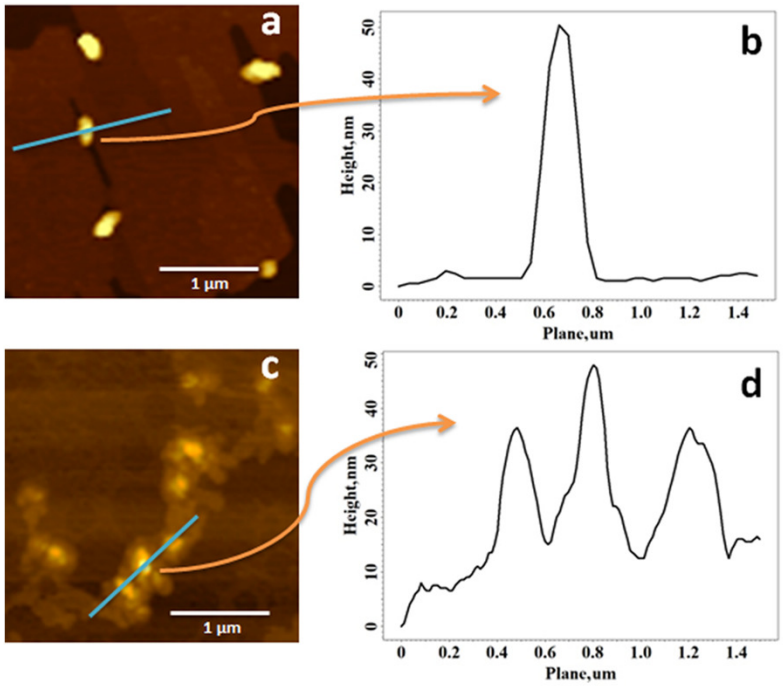


**Figure 9**. AFM images of **3** (a,b) and **3·TMe-βCD** (c,d) thin films prepared by drop-casting from THF solution.

## Electrochemical properties

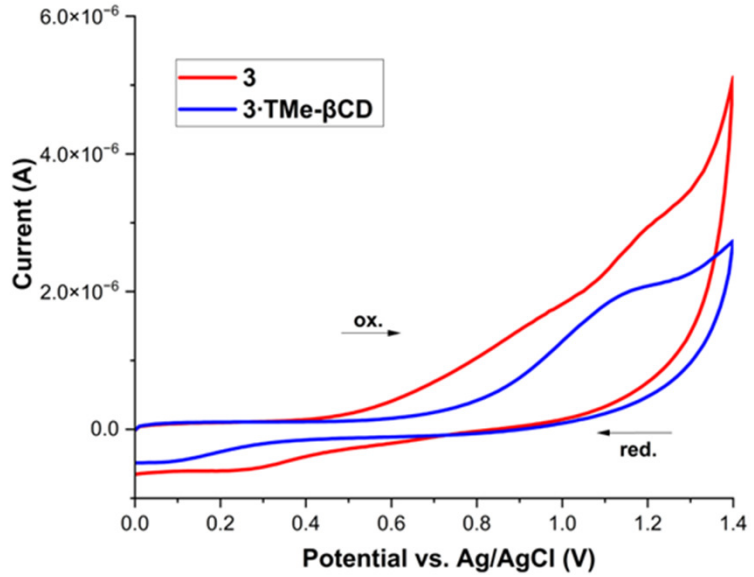


**Figure 10**. CV curves of **3** (red) and **3·TMe-βCD** (blue) in the anodic region, registered at 50 mV·s-1.

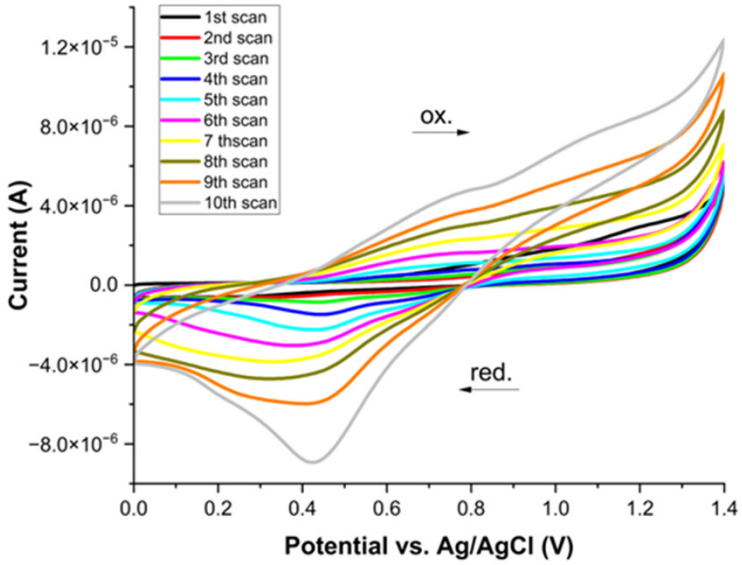


**Figure 11**. Repetitive 10 CV scans of 3 in the anodic region registered at 50 mV·s-1.

## Surface pressure-area isotherms and BAM studies of 3 and 3·TMe-βCD monolayers

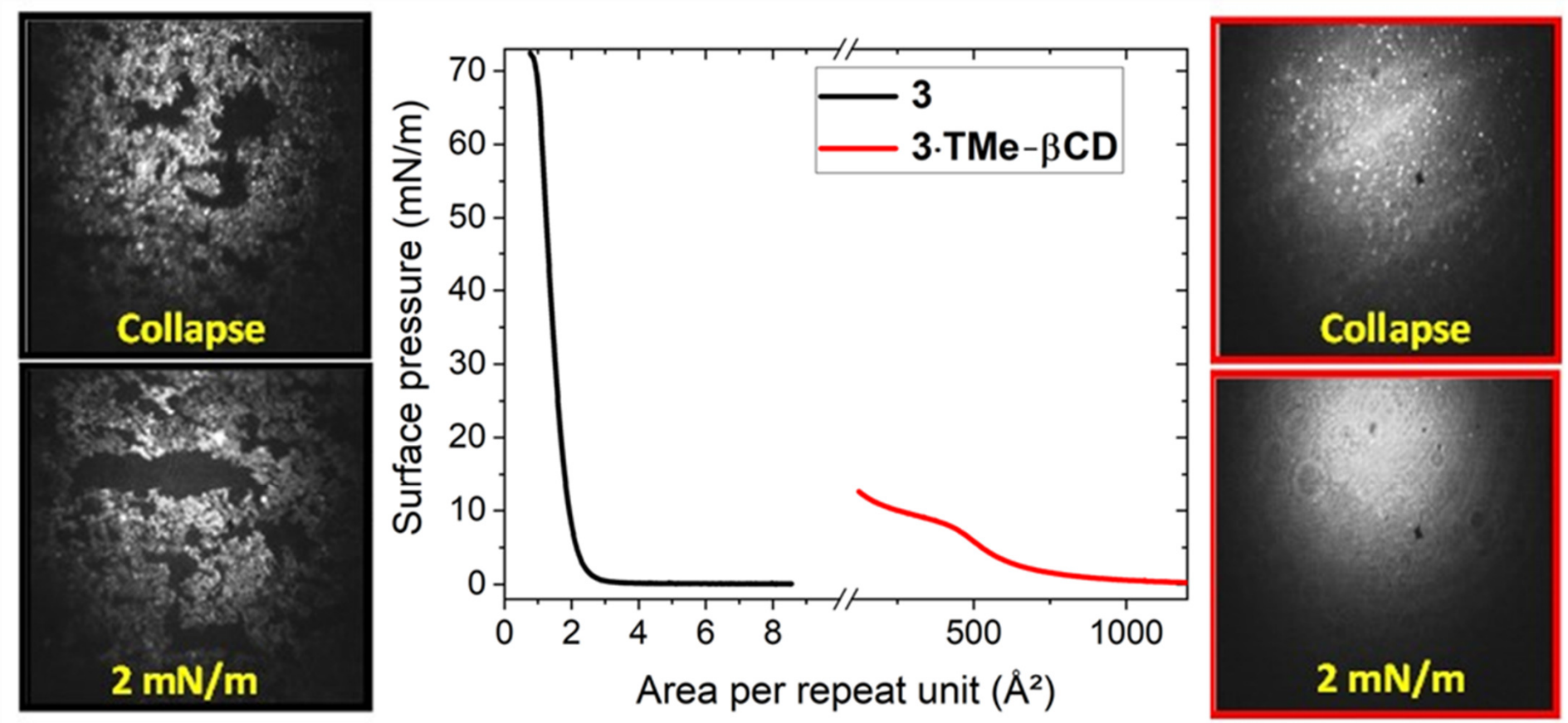


**Figure 12**. Compression isotherms and BAM images (600 µm x 600 µm) of **3** (black frame) and **3·TMe-βCD** (red frame) monolayers at 2 mN·m-1 and in the collapsed phases.

## W3.3. Sinteza polirotaxanilor si a polimerului de referinta

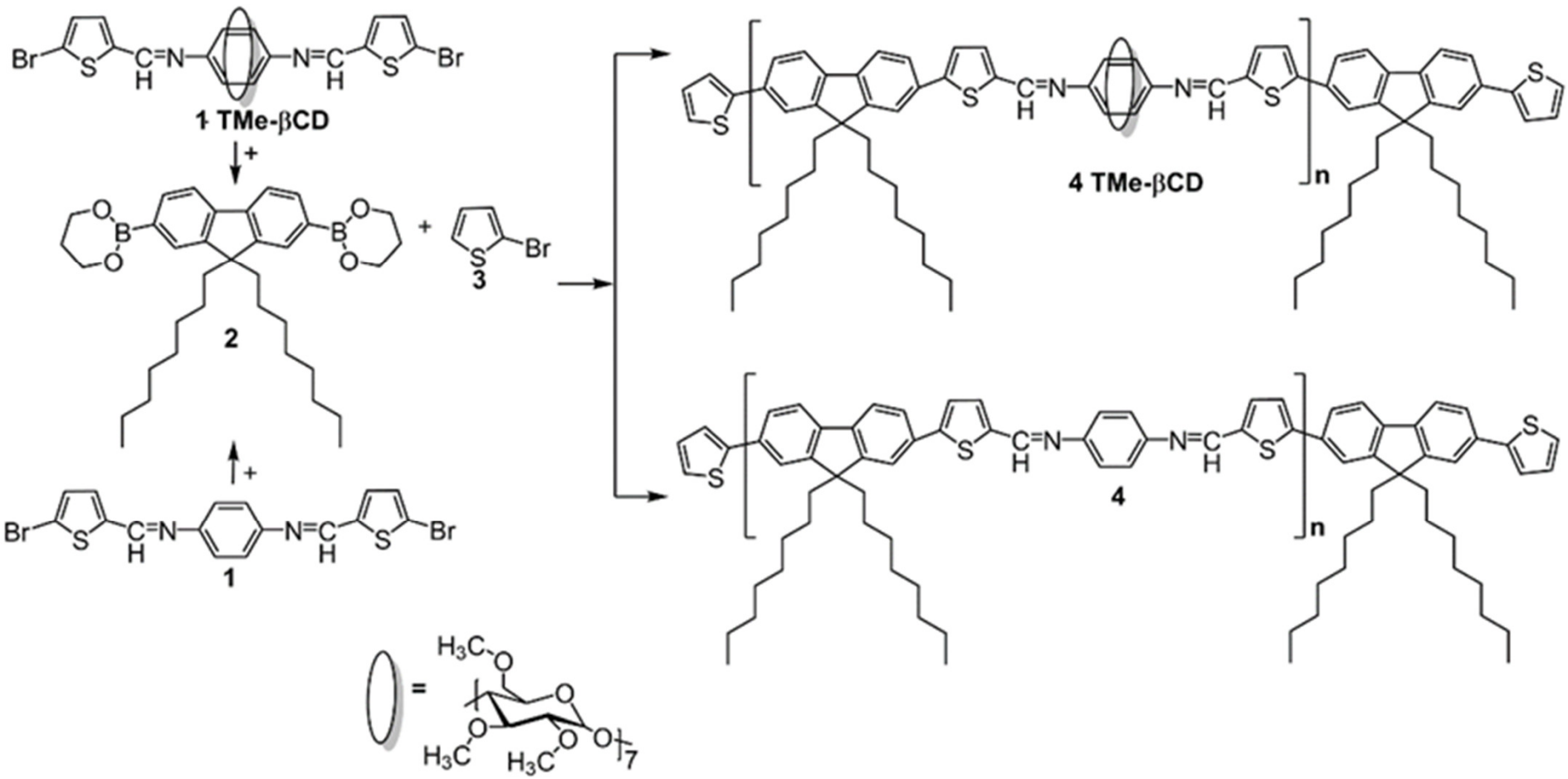


**Scheme 2**. Synthesis protocol of **4·TMe-βCD** and **4** bisazomethine-based copolymers.

# Structural characterizations

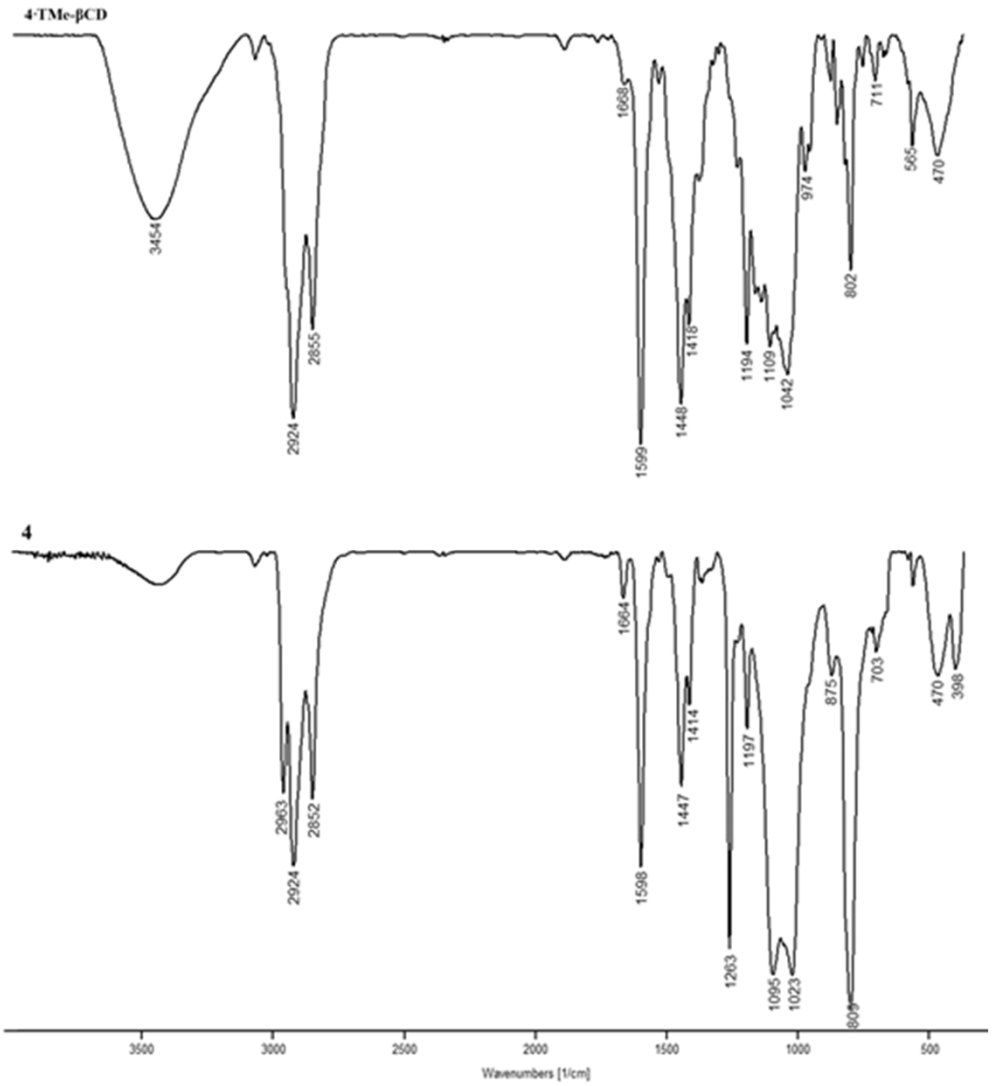


**Figure 13**. FT-IR spectra of **4·TMe-βCD** and **4**.

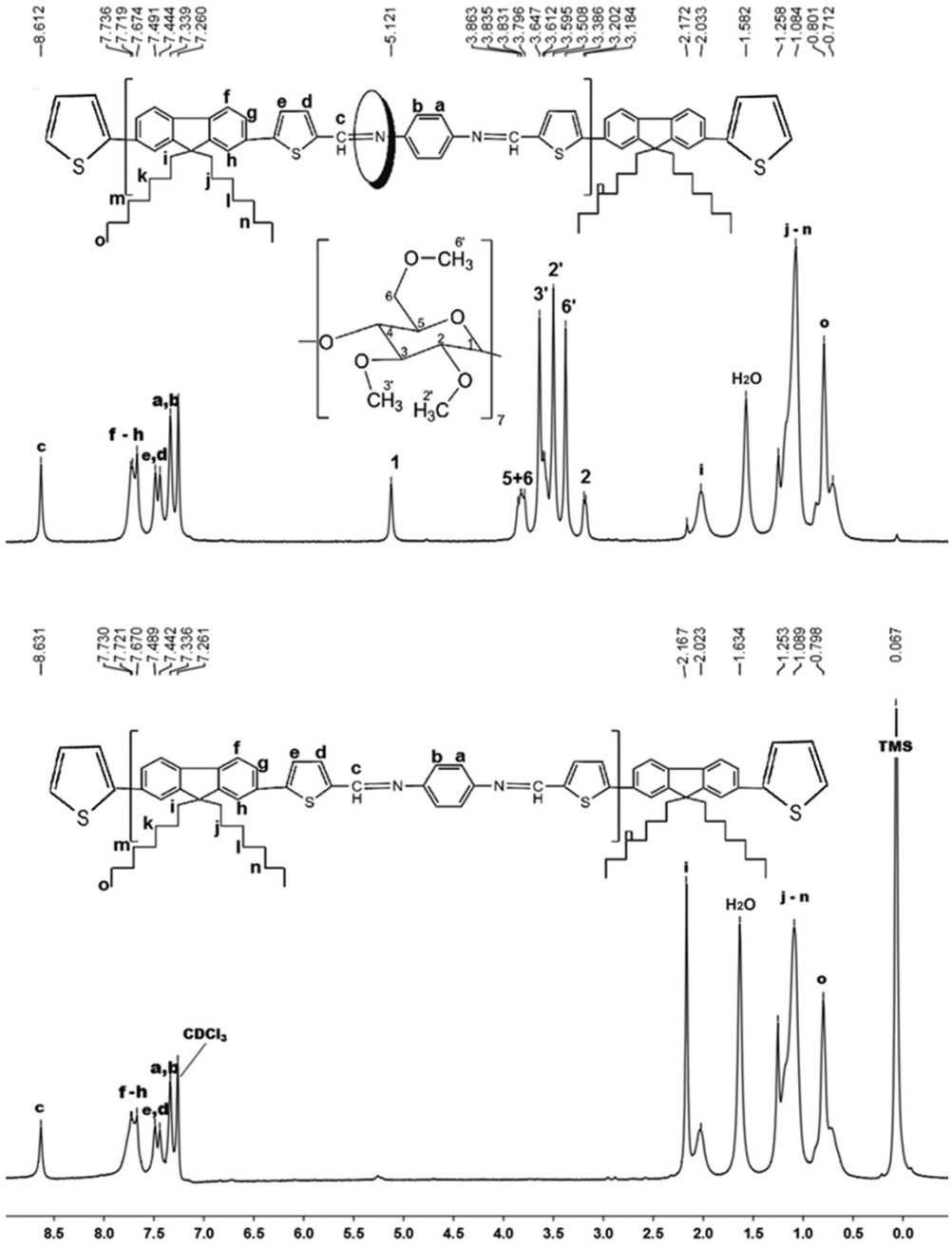


**Figure 14**. 1H-NMR spectra of the 4·TMe-βCD (top) and 4 (bottom) in CDCl3.

# The surface morphology

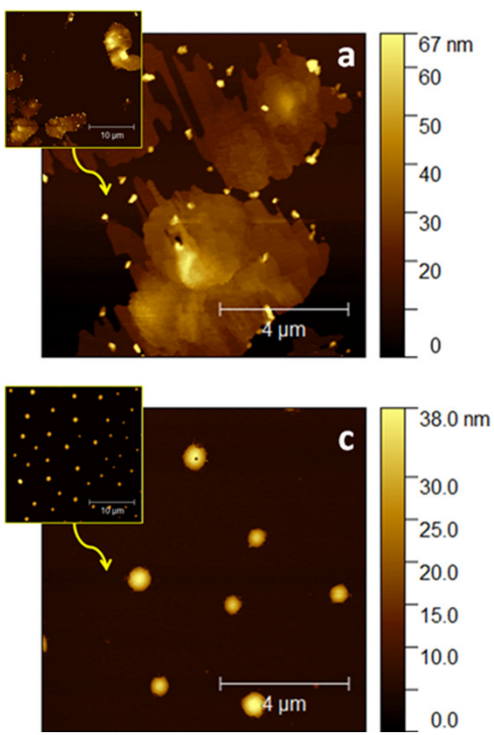


**Figure 15**. AFM images of **1** (a,b) and **4** (c,d) thin films prepared by drop-casting from THF solution in concentrated and dilute regimes, respectively.

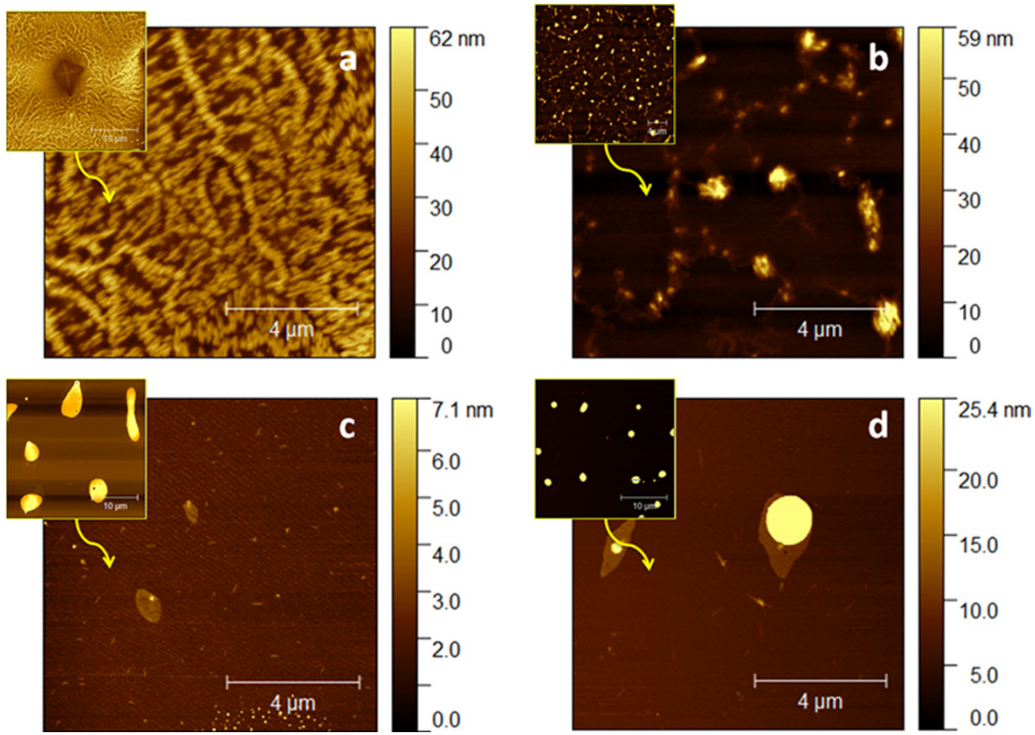


**Figure 16**. AFM images of **1·TMe-βCD** (a,b) and **4·TMe-βCD** (c,d) thin films prepared by drop-casting from THF solution in concentrated and dilute regime, respectively.

# Optical Properties

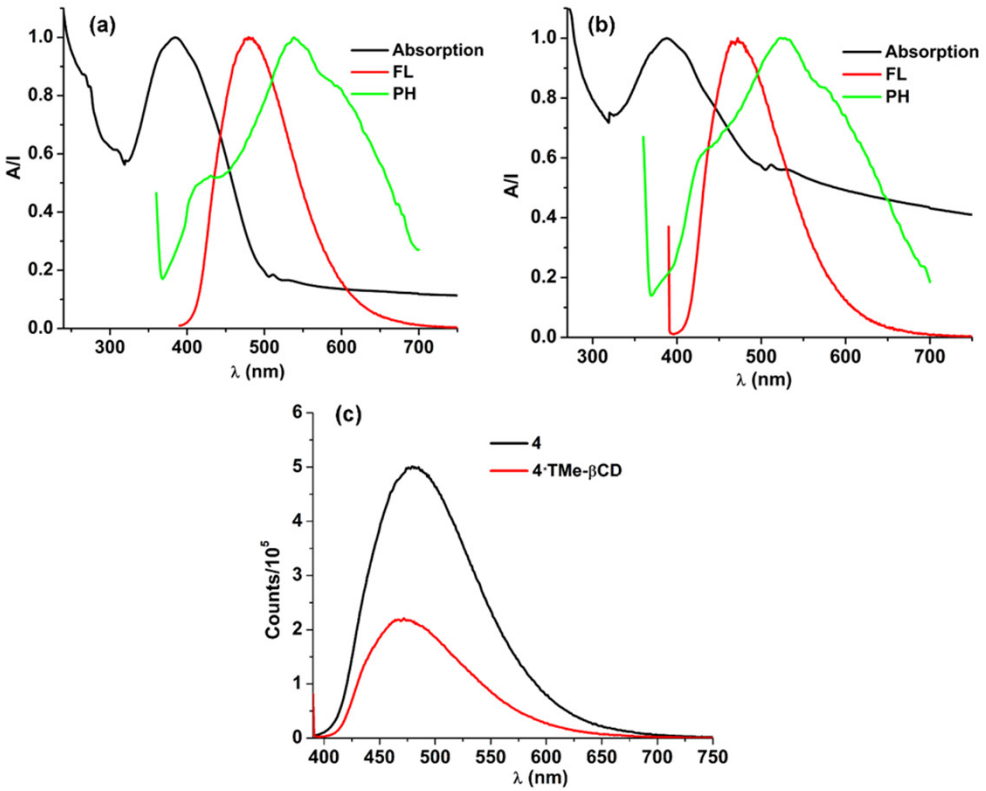


**Figure 17**. UV-Vis absorption, fluorescence and phosphorescence spectra of **4** (a) and **4·TMe-βCD** (b) and fluorescence spectra of **4** and **4·TMe-βCD** (c) at λex = 375.

| Sample | $\lambda_{ex}$ (nm) | $\lambda_{em}$ (nm) | $\tau_1$ (ns) | $\tau_2$ (ns) | $\Phi_{FL}$ (%) | $\Phi_{Ph}$ (%) |
|---|---|---|---|---|---|---|
| **4** | 375 | 483 | 1024.37(62.92%) | 8743.53(37.08%) | 13.41 | 11.75 |
| **4·TMe-βCD** | " | 472 | 1126.55(67.67%) | 9275.79(32.33%) | 22.03 | 46.76 |

**Table 1**. Emission lifetimes (τ) and chi-squared (χ2) determined by nanosecond transient absorption, and quantum yields for fluorescence (ΦFL) and phosphorescence (ΦPh) of the synthesized Schiff bases **4** and **4·TMe-βCD** in ACN.

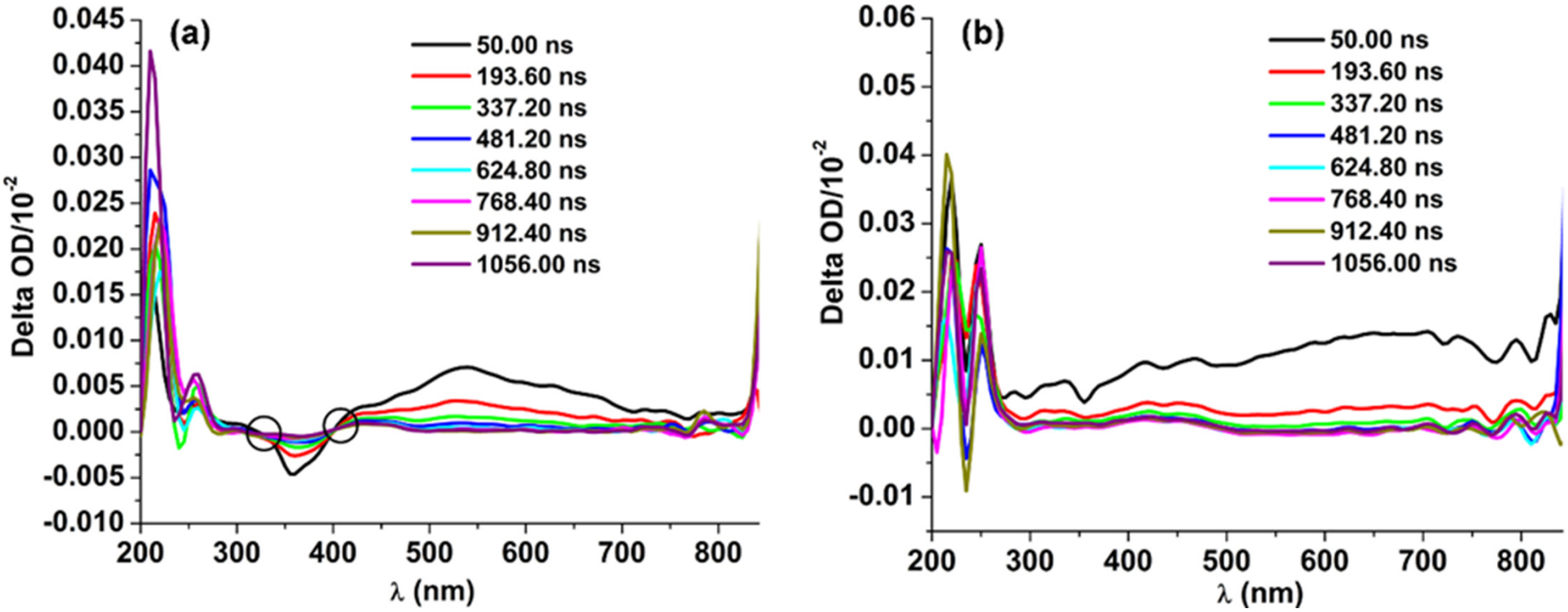


**Figure 18.** Nanosecond transient absorption maps of **4** (a) and **4·TMe-βCD** (b) in ACN (λex = 375 nm) (the black circle shows the isosbestic points).

## Electrochemical properties

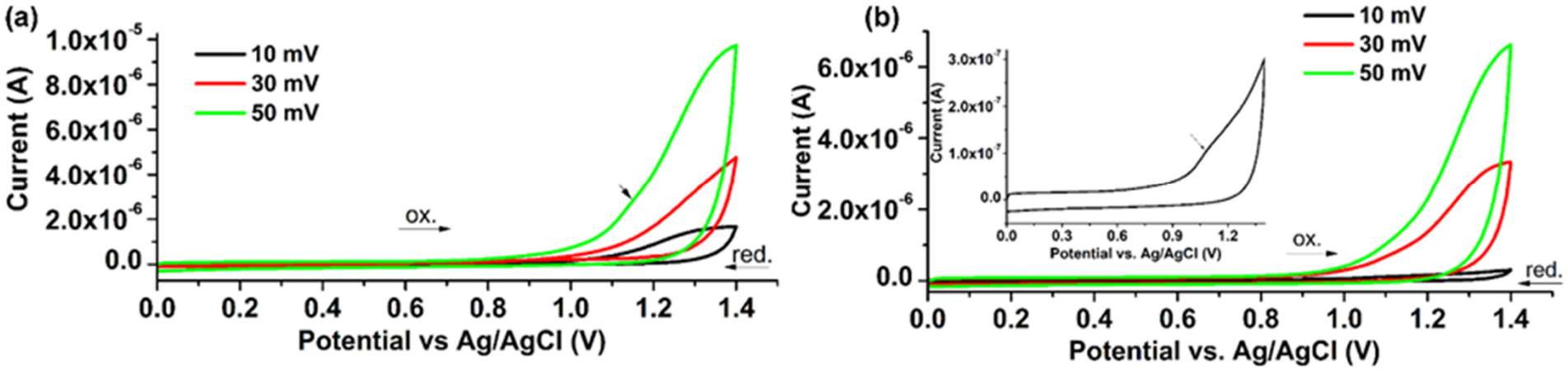


**Figure 19**. Cyclic voltammograms of fresh films of **4** (a) and **4·TMe-βCD** (b) at different scan rates, in the anodic region (inset: enlarged view of the CV curve of **4·TMe-βCD** at 10 mV·s-1).

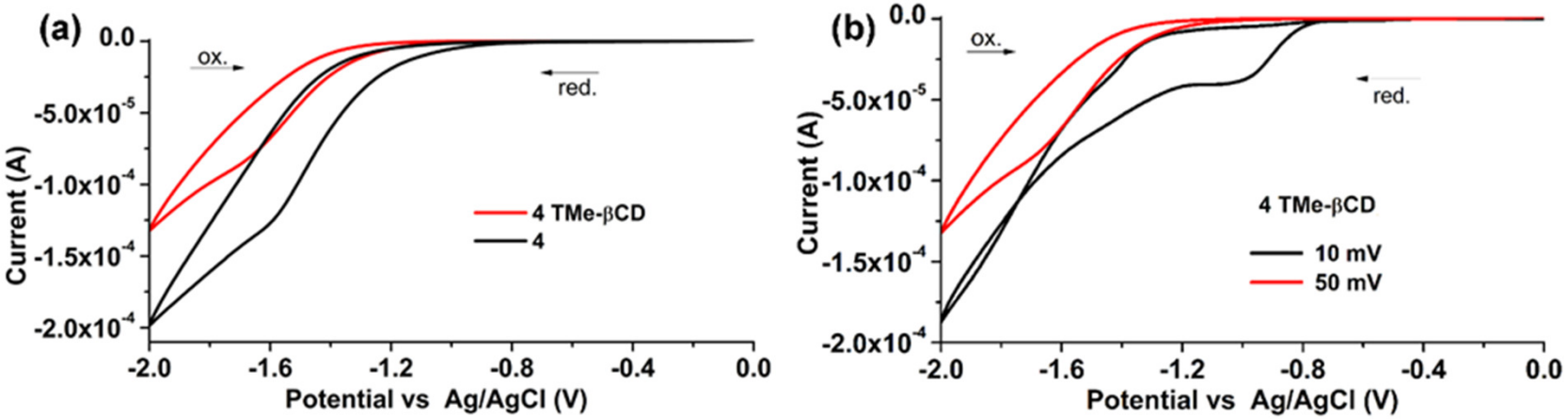


**Figure 20**. Cyclic voltammograms of **4** and **4·TMe-βCD** at 50 mV·s-1 (left) and comparative CV curves of **4·TMe-βCD** at 10 and 50 mV·s-1 (right) in the cathodic region.

## Electrical properties

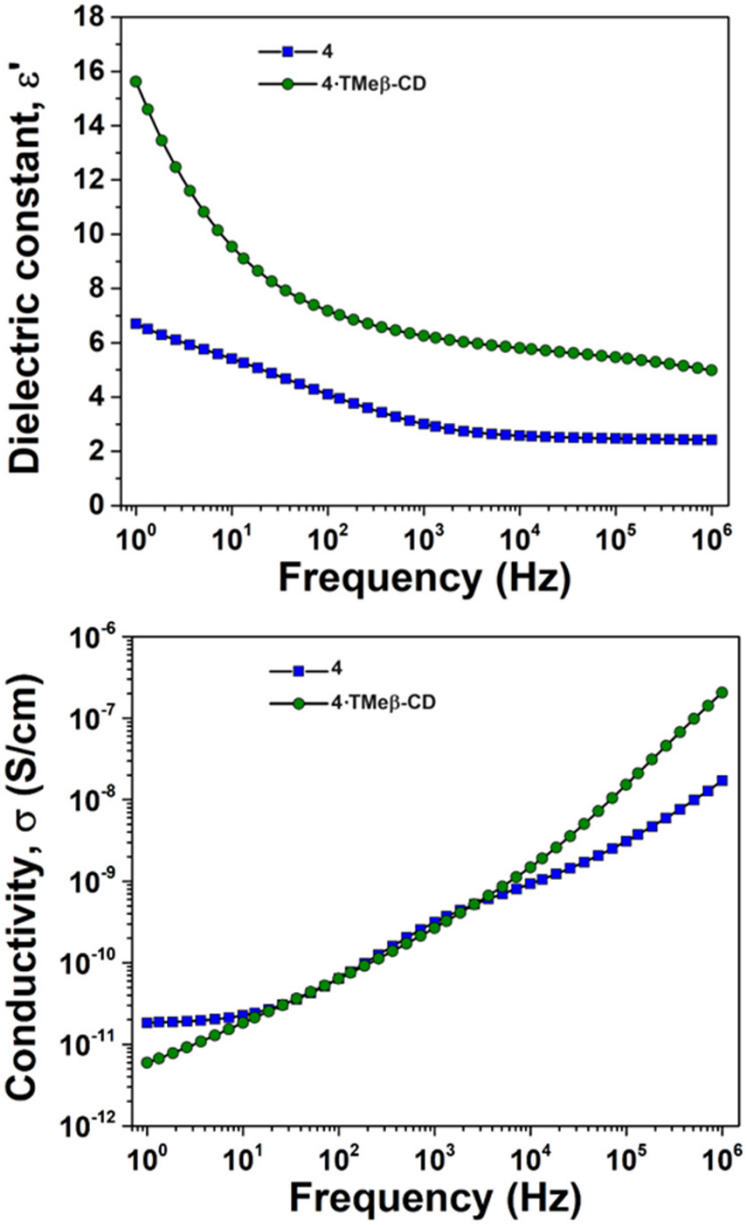


**Figure 21**. Variation of dielectric constant as a function of frequency of **4** and **4·TMe-βCD**.

**Table 2**. Electrical conductivities of **4** and **4·TMe-βCD**.

| Sample | σ (S·cm$^{-1}$)[a)] | σ (S·cm$^{-1}$)[b)] | σ (S·cm$^{-1}$)[c)] |
|---|---|---|---|
| **4** | 2.1 x 10$^{-11}$ | 7.3 x 10$^{-10}$ | 8.5 x 10$^{-7}$ |
| **4·TMe-βCD** | 6.2 x 10$^{-12}$ | 8.1 x 10$^{-11}$ | 2.2 × 10$^{-8}$ |

a)Conductivity measured by BDS method of undoped pellets; b)Conductivity measured by the four-point method of undoped pellets; c) Conductivity measured by the four-point method of iodine-doped pellets.

**Figure 22**. The variation of σ with f under alternating electrical field of **4** and **4·TMe-βCD** samples.

## Surface pressure-area isotherms and BAM studies of Langmuir monolayers

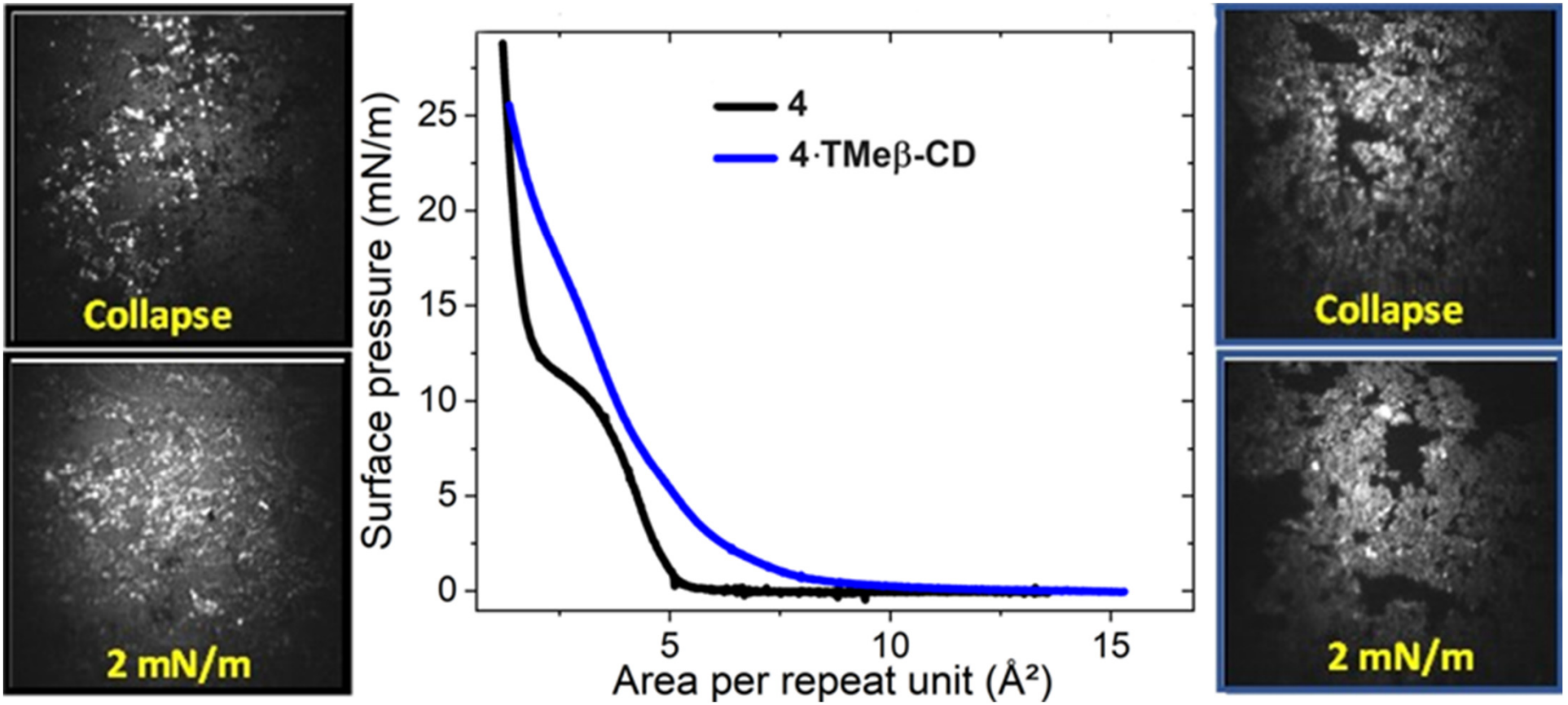


**Figure 23.** Compression isotherms and BAM images (600 µm x 600 µm) of **4** (black frame) and **4·TMe-βCD** (blue frame) monolayers at 2 mN·m-1 and in the collapsed phases.

# Diode fabrication

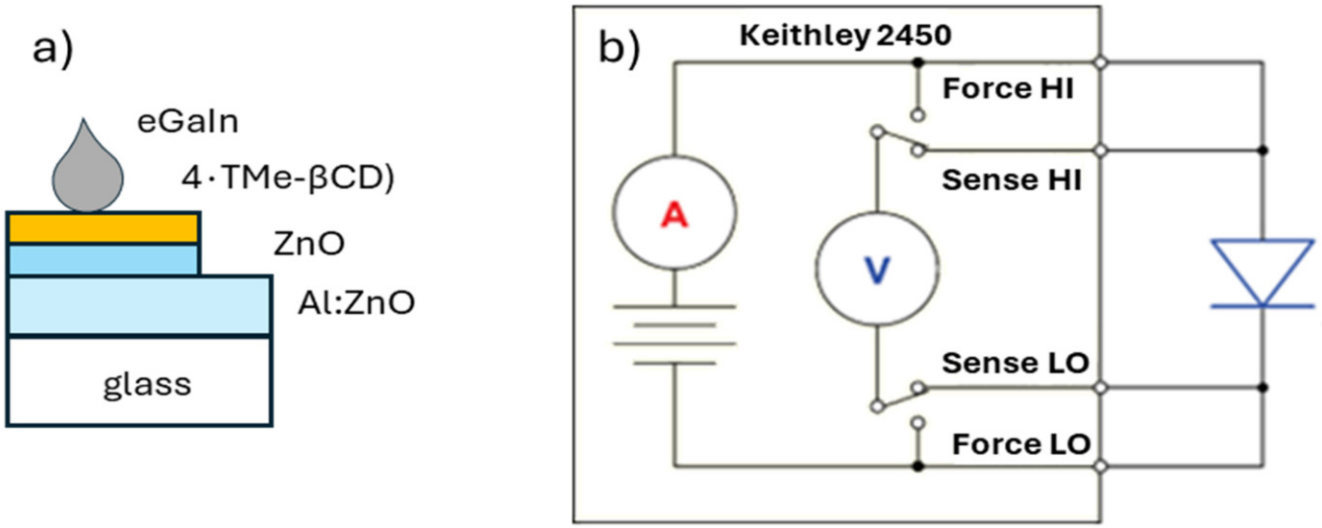


Manufactured prototype diode structure (a) and schematic diagram used to connect the source measurement unit to the diode in a 4-wire configuration (b).

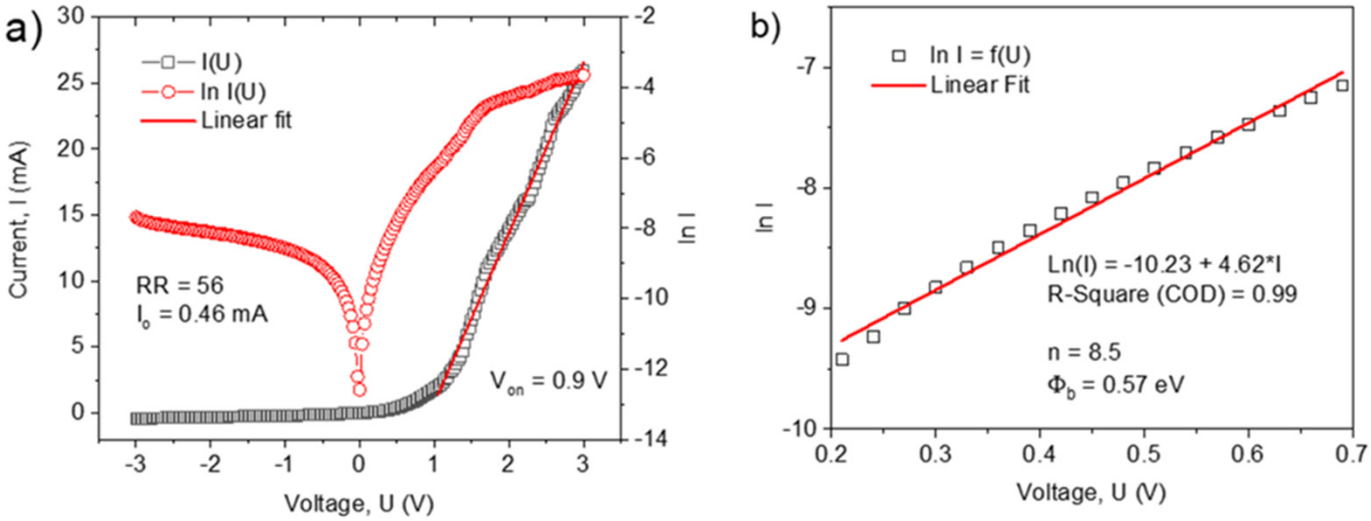


This value is quite close to conventional diodes and similar to the reported values for hybrid diodes found in the literature

Measured current-voltage characteristic of the eGaIn/4TMe-βCD/ZnO/Al:ZnO manufactured diode: a) the nonlinear current-voltage characteristic I=f(U); and b) the representation of the linear region from the semilogarithmic plot.

## Preliminarily photovoltaic results of 4·TMeβCD and 4

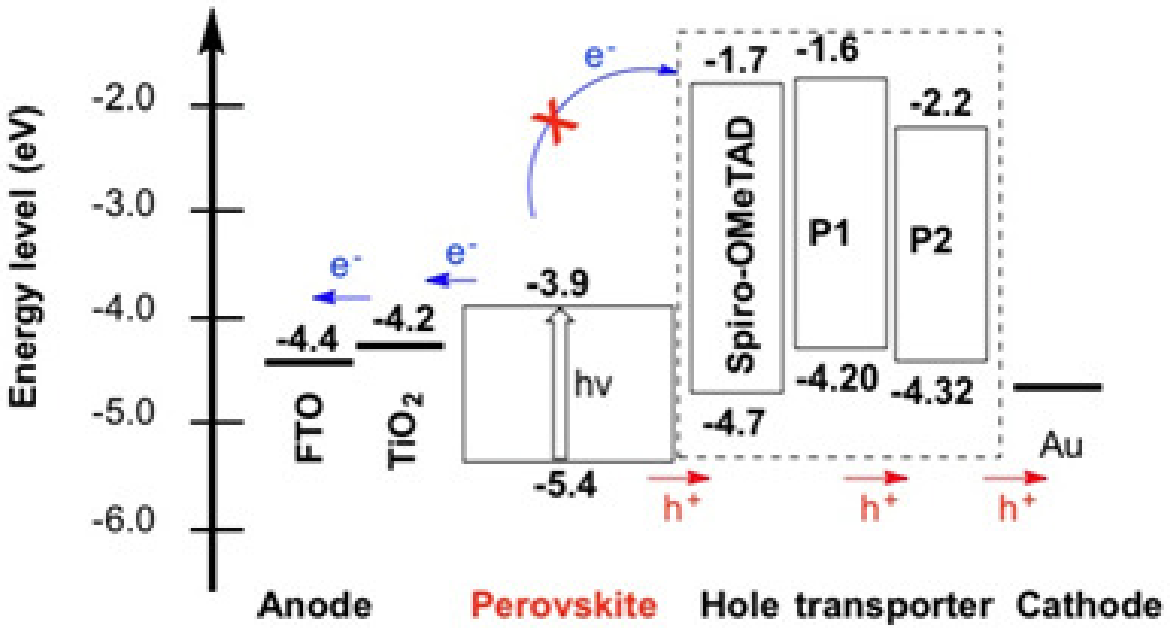


**Figure 23**. Energy level alignment of different device components.

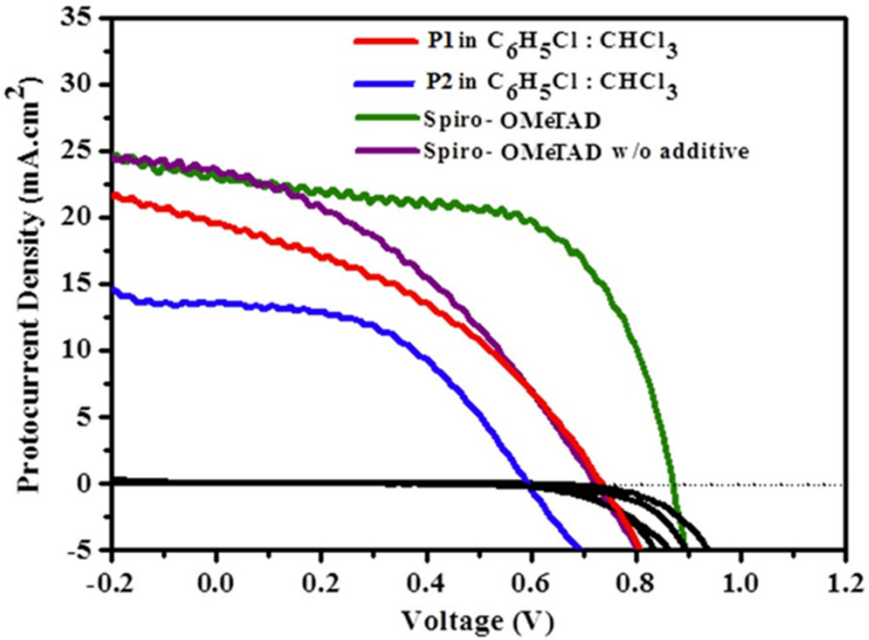


**Figure 24**. J-V curves of **P1** (**4·TMeβCD**-red) and **P2** (**4**-blue).

# Dissemination - 2024

**ISI published papers: 3**

**1**. B. Hajduk , P. Jarka, H. Bednarski , H. Janeczek , P. Kumari , A. Farcas, Thermal transitions and structural characteristics of poly(3,4-ethylenedioxythiophene/cucurbit[7]uril) polypseudorotaxane and polyrotaxane thin films, Materials 2024, 17, 1318. https://doi.org/10.3390/ma17061318

**2**. A.-M. Resmeriţă, M. Asăndulesa, A. Farcaş, Composite materials based on slide-ring polyrotaxane structures for optoelectronics, J. Polym. Sci. 2024, 1-11. https://doi.org/10.1002/pol.20240285

**Submmited: 1**

1. A.-M. Resmerita, C. Cojocaru, M.-D. Damaceanua, M. Balan-Porcarasu, S. Shova, A. El Haitami, A. Farcas, A thiophene-based bisazomethine and its inclusion complex with permethylated β-cyclodextrin: Exploring structural characteristics and computational chemistry models (DYPI-D-24-00645R1)

**Plenary conferences: 3**

**1**. A. Farcaş, Supramolecular encapsulation of semiconductors as a promising approach to organic electronic materials, Semiconductor Materials Forum -SEMICONFORUM2024, 11-15 august/2024, Madrid-Spania. https://www.continuumforums.com/2024/semiconforum

**2**. A. Farcaş, A.-M. Resmeriţă, SUPRAMOLECULAR SEMICONDUCTORS TOWARD ORGANIC ELECTRONIC MATERIALS, PolyChar World Forum on Advanced Materials
30th Edition, September 11 - 13, 2024, Iasi -Romania

**3**. A. Farcaş, SUPRAMOLECULAR ORGANIC SEMICONDUCTORS: RECENT ADVANCES AND PERSPECTIVES FOR OPTOELECTRONICS, CNCHIM2024 NATIONAL CONFERENCE OF CHEMISTRY. XXXVII EDITION, September 25-27, 2024,Targoviste-Romania

**Other:**

**1**. A. Farcaş - Program Committee, KEYNOTE SPEAKER at the Semiconductor Materials Forum - SEMICONFORUM2024, 11-15 august/2024, Madrid-Spania.
https://www.continuumforums.com/2024/semiconforum